Int. J. Heat Mass Transfer. Vol. 34, No. 8, pp. 2019–2027, 1991
Printed in Great Britain

0017-9310/91 $3.00+0.00

Instantaneous local heat transfer and hydrodynamics in a circulating fluidized bed

R. L. WU, C. J. LIM, J. R. GRACE and C. M. H. BRERETON
Department of Chemical Engineering, University of British Columbia, Vancouver, B.C., Canada V6T 1W5

(*Received* 16 *November* 1989 *and in final form* 20 *September* 1990)

Abstract—Local heat transfer mechanisms and hydrodynamics are studied in a 9.3 m tall, 152 mm i.d. transparent cold model circulating fluidized bed for 171 μm Ottawa sand. Instantaneous measurements at the wall are made with platinum-coated heat transfer probes. For some conditions, simultaneous local voidages are determined using a capacitance probe. Results show that the sudden and dramatic peaks in the measured instantaneous heat transfer coefficients are directly caused by the arrival of strands of particles at the heat transfer surface. Analyses of the capacitance probe signals indicate that these strands possess wide distributions of voidages which vary with the local time-averaged area-averaged suspension density. Simultaneous heat transfer probe measurements further suggest the existence of characteristic residence lengths for these strands. The average falling velocity of the strands is 1.26 m s^{-1} using high-speed cinematography.

INTRODUCTION

WHILE circulating fluidized beds continue to gain in popularity, especially for gas–solids reactions like combustion, fundamental understanding in critical areas like heat transfer and hydrodynamics remains seriously inadequate [1, 2]. For reliable design, modelling, and scale-up of circulating fluidized beds, it is important to know the underlying mechanisms involved in the heat transfer between gas–solids suspensions and cooling surfaces which are usually in the form of membrane waterwalls. Turndown of circulating fluidized bed boilers, for instance, is commonly achieved by varying the suspension density in the reactors. Moreover, advances in the modelling of heat transfer in circulating fluidized beds also depend heavily on a better understanding of the fundamental mechanisms involved.

Although it is obvious that there exists a close relationship between heat transfer and hydrodynamics in circulating fluidized beds, no studies have been published in this area. In this paper, we present a comprehensive study of the heat transfer mechanism in a cold model circulating fluidized bed and its relationship with the local hydrodynamics. Important hydrodynamic parameters like the strand falling velocity and residence length of strands, both of which affect the heat transfer process, are also examined.

EXPERIMENTAL EQUIPMENT

Circulating fluidized bed

All experimental data reported here were obtained in the cold model circulating fluidized bed unit shown in Fig. 1 and described previously in refs. [3, 4]. It consists of a riser, a storage column, an L-valve, and two cyclones. Except for the two cyclones, the entire unit is constructed of 6.4 mm thick transparent polyacrylic material (Plexiglas) for easy visual hydrodynamic observation.

The riser column is 9.3 m tall and has a 152 mm i.d. Solid particles in the riser are entrained in the fast fluidization regime by air introduced to the bottom of the column through a perforated plate distributor. Particles carried out of the riser are captured by pri-

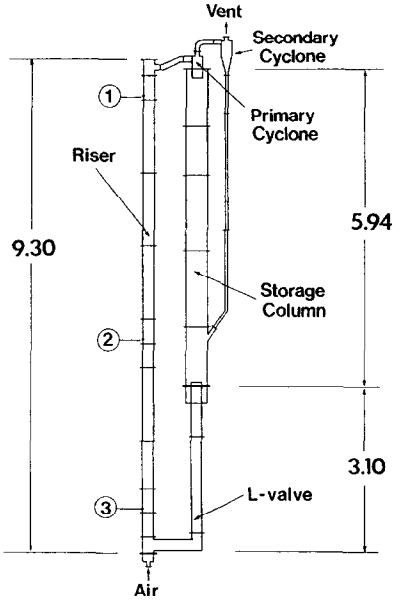

FIG. 1. Schematic of the cold model circulating fluidized bed. All dimensions are in m.

NOMENCLATURE

a separation distance between two heat transfer probes [m]
a_{int} length defined in equation (1) [m]
a_{tan} value of a where tangent to r_{max} vs a curve (e.g. Fig. 11) at $a = 0$ intersects a-axis [m]
$a_{0.5}$ value of a corresponding to $r_{max} = 0.5$ on r_{max} vs a curve (e.g. Fig. 11) [m]
$A_1, A_2, \ldots, A_8$ areas defined in Fig. 7 [m^2]
f time fraction of wall coverage by strand
$f_1, f_2, \ldots, f_5$ wall coverage time fractions defined in Fig. 7
G_s circulation flux of solids [kg m^{-2} s^{-1}]
h_i instantaneous heat transfer coefficient [W m^{-2} K^{-1}]
r cross-correlation coefficient
r_{max} maximum cross-correlation coefficient for a given set of conditions
r_0 limiting value of r at large a (see Fig. 11).

Greek symbols
ε local voidage of strand near the wall
ρ_{susp} suspension density at a given level averaged over column cross-section and derived from vertical profiles of static pressure [kg m^{-3}]

mary and secondary cyclones and are recirculated via a 5.94 m tall, 343 mm i.d. storage column and an L-valve to the bottom of the riser. The rate of recirculation of solids, G_s, is controlled by adjusting the aeration just above the vertex of the L-valve and is measured by tracking particles in the downflow leg of the L-valve and assuming plug flow across the section. Suspension densities of solids in the riser are estimated from the pressure profiles obtained along the column assuming accelerational and frictional terms to be negligible, as in most circulating fluidized bed studies. Particles used in the experiments were Ottawa sand of surface-volume mean diameter 171 μm. The size distribution and other key fluidization properties of the particles are given in Table 1.

Instantaneous heat transfer probes

The instantaneous heat transfer probes consisted of thin platinum films deposited on pieces of glass of area approximately 10 × 10 mm. Fabrication, calibration, and operation procedures have been described in detail in refs. [4, 5]. In brief, each platinum film is first bonded to its glass support by curing a piece of glass coated with platinum solution in a 650°C oven. It is then connected to a programmable power supply and a known reference resistor. Figure 2 shows the probe circuit designed to measure instantaneous heat transfer coefficients. The platinum film functions simultaneously both as a heater element and a temperature sensor. Its temperature is maintained constant and the instantaneous power dissipation from the probe is measured by means of an IBM XT Personal Computer coupled with an A/D–D/A interface board (Tecmar Labmaster TM-40).

The probe is mounted at one end of a guard heater with its surface flush with the inner wall of the column, as shown in Fig. 3. The guard heater minimizes the heat loss from the back of the probe and limits the temperature variations of the glass support. A 10 μm thick plastic film is used to cover the platinum film to protect it from wear due to the particles. The response time of the probe assembly shown in Fig. 3 was determined experimentally [5] to be about 45 ms.

Table 1. Particle size analyses and fluidization properties for Ottawa sand

Size range (μm)	Percentage weight (%)
707–500	0.1
500–354	2.3
354–250	14.6
250–177	43.6
177–125	27.5
125–88	6.9
88–53	3.0
53–44	1.2
44–0	0.8
Mean particle size (μm)	171
Particle density (kg m^{-3})	2650
Calculated terminal settling velocity for mean size at room temperature and pressure (m s^{-1})	0.99
Minimum fluidization velocity at room temperature and pressure (mm s^{-1})	31
Voidage at minimum fluidization	0.43

Capacitance probe

A capacitance probe was used in some of the experiments to measure the local instantaneous con-

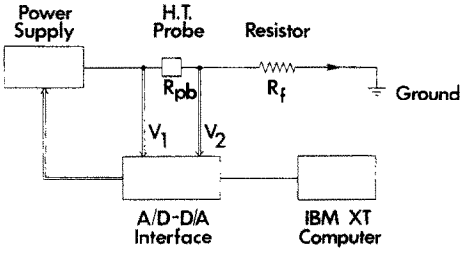

FIG. 2. Schematic of the circuit for controlling the temperature of the heat transfer probe and measuring the instantaneous heat transfer coefficients.

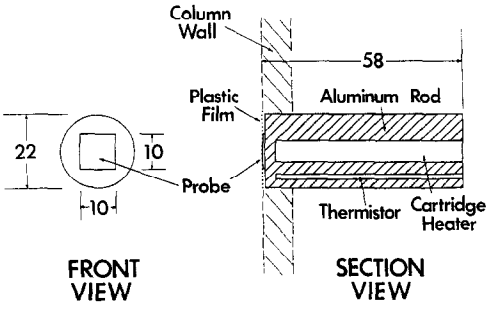

FIG. 3. Front and section views of the probe assembly consisting of plastic film, platinum-coated glass, and guard heater. All dimensions are in mm.

centration of solids in the vicinity of the heat transfer probe. This capacitance probe was adapted directly from one used in previous work in this department [3], but with an extended length.

The capacitance probe design is shown in Fig. 4. The probe sheath is constructed from 6.4 mm o.d., 4.6 mm i.d. stainless steel tubing. At one end of the sheath, a 3.2 mm o.d., 2.2 mm i.d. stainless steel tubing is press-fitted into a 6.4 mm o.d. bushing to project 20 mm beyond the sheath and form the probe tip. The live probe component, made of a 0.6 mm diameter, rigid, single strand, stainless steel wire, protrudes 4 mm from the sheath at the probe tip. This wire is held rigid and insulated from the sheath by a single, continuous, magnesium oxide, thermocouple insulator which is in turn held rigid in the sheath using ceramic cement. The wire is connected to a BNC coaxial coupling at the other end of the sheath.

Figure 4 also shows the equivalent circuit of the capacitance probe. This consists of a fixed capacitance between the shielded wire and the grounded 6.4 and 3.2 mm sheaths, and a variable capacitance between the exposed live tip and the closest 2–3 mm of the grounded 3.2 mm sheath. Field lines radiate out from the live tip to this grounded area forming a capacitance which varies when solids, with dielectric constant different from air, pass through the field. The capacitance change is detected by making the probe part of an LC circuit for which the resonant frequency is a measure of the probe capacitance; this is typically approximately 5 MHz. The LC circuit is made to resonate by an oscillator and the resonant frequency is then measured. A commercially available reactance conversion system, the Disa 51EO1 reactance converter, combined with a type 51EO2 oscillator and 51EO2 tuning plug, is used in the capacitance probe circuit, and has proved capable of measuring signals up to a frequency of 100 kHz. The output from the capacitance probe, also recorded using a Tecmar interface board, is a nearly linear function of the voidage in the measurement zone for voidages from 0.5 to 1.0 and is insensitive to the distribution of solids in the measurement zone.

High-speed cinematography

For some experimental conditions, the hydrodynamics at the column wall were recorded with the aid of high-speed movies taken primarily for analyzing the movement of the waves of particles or strands at the column wall. A high-speed camera (Hycam Model 400) and 16 mm black-and-white movie film (Kodak 7277 4X reversal film) were used together with appropriate front lighting. The speed used for all films was 400 frames per second.

RESULTS AND DISCUSSIONS

Simultaneous heat transfer probe and capacitance probe experiments

In the first part of this study, simultaneous measurements were made with an instantaneous heat transfer probe and a capacitance probe, both located 3.74 m above the distributor. The capacitance probe was inserted into the column from a port diametrically

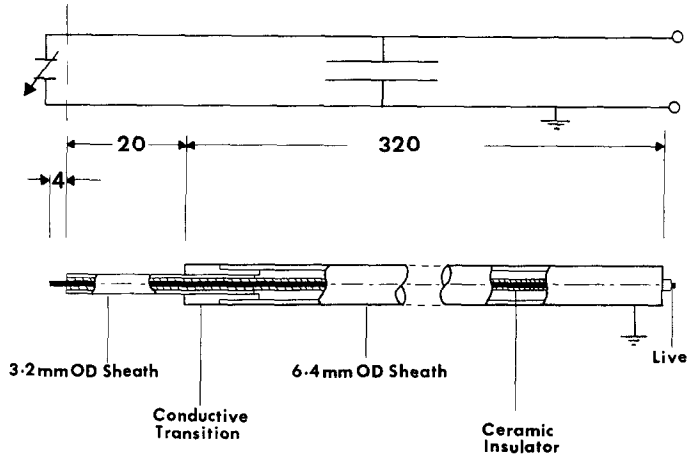

FIG. 4. Schematic of capacitance probe and its equivalent circuit. All dimensions are in mm. A region around the 4 mm length of exposed wire and the 3.2 mm o.d. sheath at the left forms the measurement volume. On the right-hand end, the probe is connected to the rest of the LC circuit.

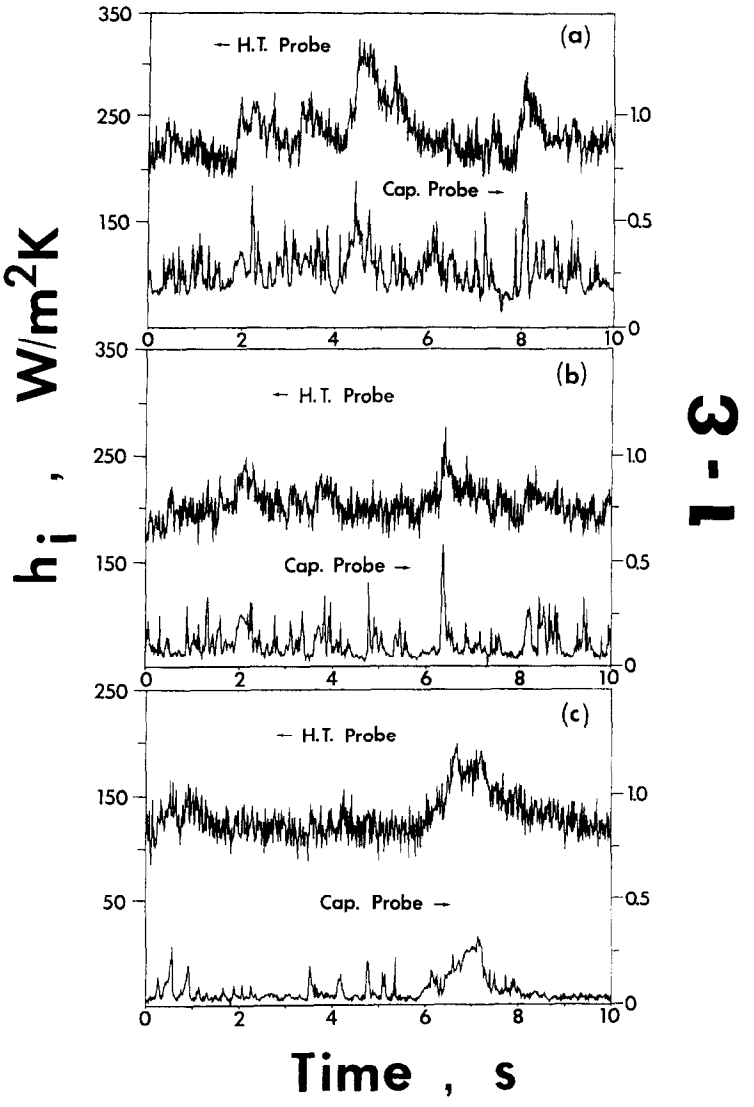

FIG. 5. Typical traces of simultaneous instantaneous heat transfer coefficient and capacitance signal at three different cross-sectional area-averaged suspension densities (kg m^{-3}): (a) 46.7; (b) 32.0; (c) 15.3. G_s (kg m^{-2} s^{-1}): (a) 62.8; (b) 49.7; (c) 35.2.

opposite the heat transfer probe such that the tip of the probe wire came within 1 mm of the heat transfer probe surface. Data were obtained for area-averaged suspension densities from 15 to 47 kg m^{-3} at a superficial gas velocity of 7 m s^{-1}. Figure 5 shows some typical simultaneous traces of both heat transfer and capacitance probe signals at three different cross-sectional area-averaged suspension densities. The heat transfer traces show sudden and dramatic peaks in heat transfer coefficient for all three suspension densities, similar to the traces obtained earlier in ref. [4]. The qualitative appearance of the capacitance signals obtained are similar to those obtained in refs. [3, 6]. Comparisons of the capacitance signals with the heat transfer signals show that, in general, the capacitance probe signals show more peaks. The peaks in the capacitance signal are also more dramatic and sudden. These trends can be explained by the different response times and measuring volumes of the two probes. The fuzzier appearance of the heat transfer signal is due to the control circuit used to maintain the heat transfer probe temperature constant. Since its response time is much faster than that of the heat transfer probe (approximately 1 ms vs 45 ms), the capacitance probe revealed more details of the time variations in local concentration of solids. Also, since the capacitance probe has a smaller measuring volume than its counterpart, its signals showed more dramatic peaks due to a reduced probability of averaging of concentration of solids in its measuring volume. The occasional lack of agreement between the two signals is probably due to the fact that the measuring volumes

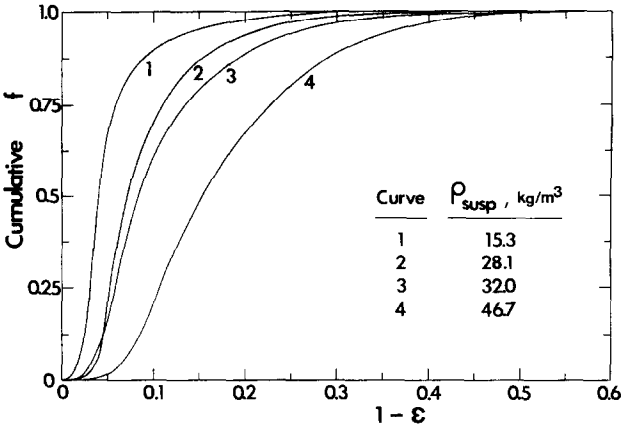

FIG. 6. Cumulative time fraction of wall coverage by strands with voidage ε (or larger) vs $1-\varepsilon$ at four different suspension densities.

of the two probes did not coincide exactly since the measuring volume of the capacitance probe does not extend more than 1 mm beyond the live wire at its probe tip [3]. Therefore, it is likely that some particle strands detected by the capacitance probe did not make contact with the heat transfer probe and cause a change in the heat transfer coefficient. Nevertheless, it is apparent from Fig. 5 that, in general, the sudden and dramatic peaks in the instantaneous heat transfer coefficient traces correspond closely with similar peaks in the capacitance traces. This suggests that the abrupt increases in heat transfer coefficient are caused by the arrivals of particle packets or strands at the surface of the heat transfer probe. It also confirms for the first time the important role of these particle strands in circulating fluidized bed heat transfer and affirms the predominance of the particle convective component, as suggested by Grace [1] and Glicksman [2]. The lowest heat transfer coefficients in Fig. 5(c) correspond to periods when few solids are detected by the capacitance probe, and the values are close to those for gas alone under similar flow conditions [4]. Figure 5 also indicates that as the cross-sectional area-averaged suspension density in the column increases, the concentration of solids in the wall region, as well as the frequency and density of the strands, also increases, causing a corresponding increase in the heat transfer coefficient.

As the majority of heat transfer surfaces in circulating fluidized beds are located on the column wall, hydrodynamic information on the wall layer of particles adjacent to the transfer surfaces is critical for understanding the heat transfer mechanisms. The capacitance probe signals obtained above contain such hydrodynamic information. Figure 6 is a cumulative frequency distribution plot of the capacitance probe signals shown in Fig. 5, in which the cumulative time fraction of wall coverage by a strand of voidage ε (or larger) is plotted against $(1-\varepsilon)$ for four cross-sectional area-averaged suspension densities. Figures 5 and 6 both indicate clearly that fast fluidized beds, unlike bubbling fluidized beds, do not possess two discrete and distinct phases (i.e. a uniform low voidage dense phase and a high voidage dilute phase), at least above the turbulent primary zone. Instead, the fast fluidized bed exhibits a wide distribution of voidages which vary with the time-averaged and cross-sectional area-averaged suspension density. In order to characterize the voltage distributions for the strands, the cumulative frequency distribution plots shown in Fig. 6 are each discretized according to the scheme shown in Fig. 7. The different time fractions of wall coverage f_1, f_2, etc., corresponding to different values of $(1-\varepsilon)$, are adjusted such that areas $A_1 = A_2$, $A_3 = A_4$, and so on. The resulting values of f and corresponding $(1-\varepsilon)$ values for four different suspension densities are shown in Table 2. The time fraction of wall coverage, f, is then plotted against suspension density at six different values of voidage in Fig. 8. This figure provides a convenient way of estimating the time fraction of wall coverage corresponding to different voidages for a wide range of suspension densities.

Double heat transfer probe experiments

Instantaneous heat transfer coefficients were next obtained simultaneously from two heat transfer probes at the wall near the middle of the height of the column at a fixed superficial gas velocity of 7 m s^{-1}.

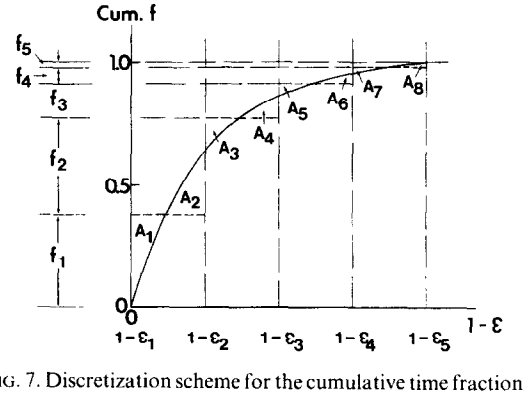

FIG. 7. Discretization scheme for the cumulative time fraction of wall coverage plots in Fig. 6.

Table 2. Time fractions of wall coverage for strands of different voidages at four suspension densities

	Suspension density (kg m^{-3})			
	15.3	28.1	32.0	46.7
$1-\varepsilon$	Time fraction of wall coverage, f			
0.0	0.525	0.271	0.232	0.050
0.1	0.423	0.581	0.547	0.421
0.2	0.041	0.116	0.157	0.326
0.3	0.011	0.023	0.047	0.139
0.4	0.0	0.009	0.017	0.050
0.5	0.0	0.0	0.0	0.014
Sum	1.0	1.0	1.0	1.0

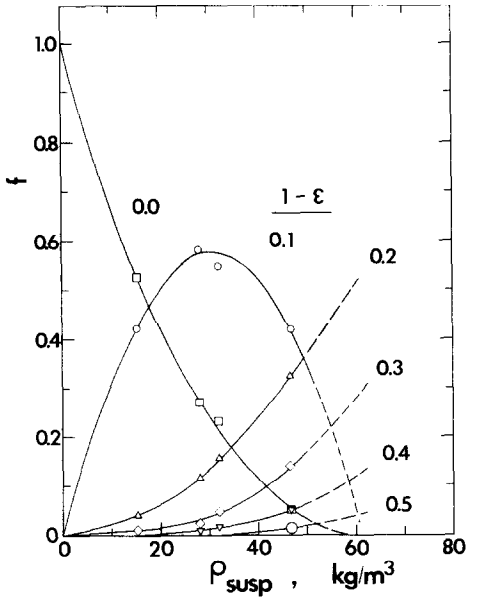

FIG. 8. Time fraction of wall coverage vs suspension density for six different strand voidages.

The upper probe was fixed at 4.34 m above the distributor and was aligned vertically with the lower probe. The distance, a, separating the two probes, was varied from 0.152 to 0.762 m at regular intervals of 0.152 m. For each distance a, simultaneous heat transfer data were obtained for three different area-averaged suspension densities ranging from about 15 to 44 kg m^{-3}. Figure 9 shows some typical simultaneous traces of the two instantaneous heat transfer coefficients. In order to determine the degree of correlation of the two traces, the simultaneous heat transfer coefficients were treated statistically using the cross-correlation procedure. A statistics software package, STATGRAPHICS, running on an IBM XT personal computer, was used to perform the cross-correlation. The calculated coefficient of cross-correlation, r, is plotted against time lag in Fig. 10 for five different separation distances and three suspension densities. It can be seen from Fig. 10 that the degree of cross-correlation decreases rapidly with increasing separation distance and with decreasing suspension density. It should be noted that since most of the profiles show a low degree of cross-correlation, caution should be used when trying to interpret these plots. However, for profiles that show some significant degree of cross-correlation (i.e. profiles 1a, 1b and 2a in Fig. 10), their relatively flat shapes indicate that there is a rather wide spectrum of velocities for the waves of particles or strands at the wall of the column. Nevertheless, the fact that the maxima of these profiles are located on the left-hand side of the time lag scale (i.e. negative time lag) indicates a predominantly downward particle velocity at the wall. This is consistent with the visual observation at the column wall where waves of particles or strands can be seen sweeping predominantly downward along the wall, with occasional upward motion interspersed. From profiles 1a and 1b, a downward strand velocity of 1.62 m s^{-1} can be estimated if the time lag corresponding to the maximum in each of the profiles is used.

The maximum coefficient of cross-correlation, r_{max}, for each of the profiles shown in Fig. 10 is plotted against the separation distance, a, for three suspension densities in Fig. 11. Since our main interest is in the downward direction, only the negative time lag scale is considered when plotting the maximum correlation coefficient. It can be seen from Fig. 11 that r_{max} decreases rapidly with increasing separation distance. Also, the rate of decrease is more pronounced with decreasing suspension density. Figure 11 suggests that the length a strand will descend at the wall depends on the cross-sectional area-averaged suspension density. The higher the suspension density, the further the strands descend at the wall before disintegrating. Moreover, it can be seen that r_{max} does not decrease to zero, but rather tends to a small base value, r_0, in all cases.

It is possible for one to estimate from Fig. 11 a 'characteristic' residence length for the strands. Three different procedures for estimating such a length can be used:

(1) $a_{0.5}$—value of a corresponding to $r_{max} = 0.5$ (see Fig. 11);

(2) a_{tan}—value of a where the tangent, drawn to the curve (Fig. 11) at $a = 0$, intersects the a-axis;

(3) a_{int} the length obtained by integrating the area bounded by the curve, Fig. 11, and $r_{max} = r_0$, or

$$a_{int} = \frac{1}{1-r_0}\int_{r_0}^{1} a\,dr_{max}. \qquad (1)$$

The three characteristic residence lengths for the strands, as defined above, are obtained for three suspension densities and plotted in Fig. 12 as a function of suspension density. It can be seen from Fig. 12 that $a_{0.5}$ and a_{int} are very similar to each other, while a_{tan} is approximately twice the magnitude of the other two. The line fitted to a_{int} in Fig. 12 can be expressed as

$$a_{int} = 0.0178\,\rho_{susp}^{0.596}. \qquad (2)$$

Since the waves of particles or strands fall mostly along the wall, it is conceivable that any roughness at the wall would significantly affect the characteristic

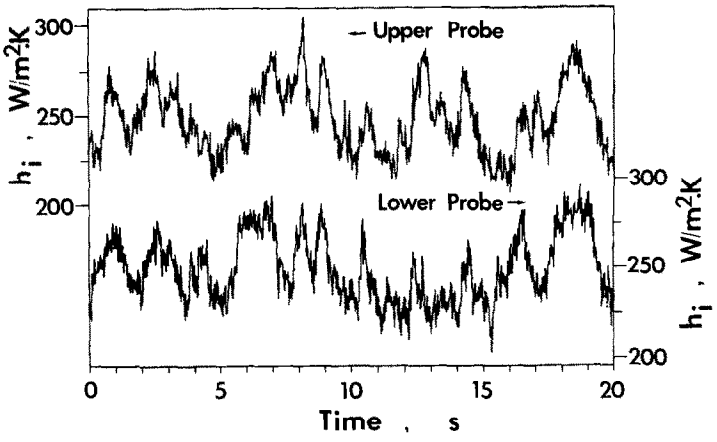

FIG. 9. Typical traces of two simultaneous instantaneous heat transfer coefficients: $a = 0.152$ m; $\rho_{susp} = 44.2$ kg m^{-3}; $G_s = 60.3$ kg m^{-2} s^{-1}.

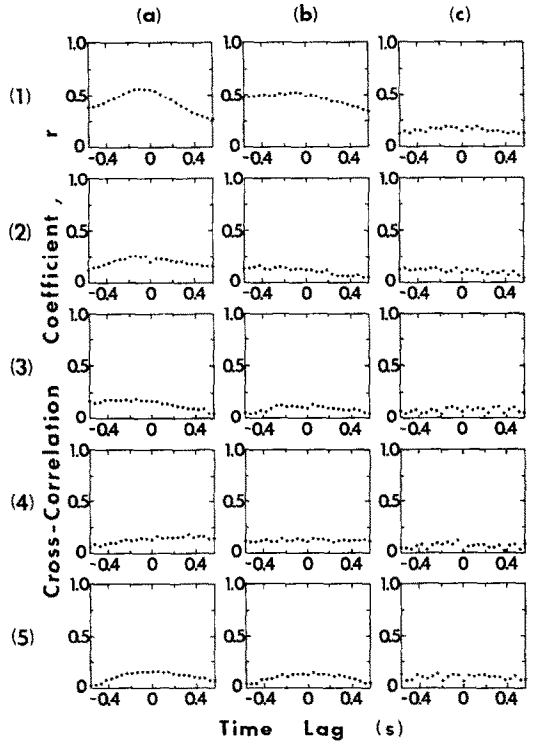

FIG. 10. Coefficient of cross-correlation vs time lag at three different suspension densities and five separation distances. Probe separation distance (m): (1) 0.152; (2) 0.305; (3) 0.457; (4) 0.610; (5) 0.762. ρ_{susp} (kg m^{-3}): (a) 44.2; (b) 28.7; (c) 14.8.

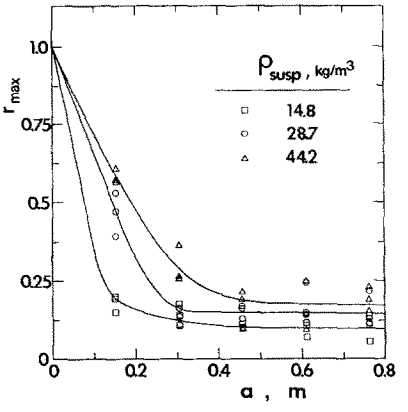

FIG. 11. Maximum cross-correlation coefficient vs separation distance at three different suspension densities.

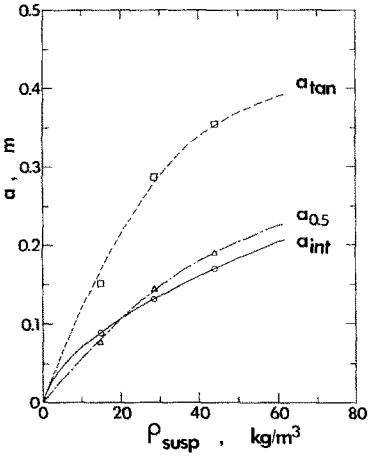

FIG. 12. Variations of $a_{0.5}$, a_{tan}, and a_{int} as a function of suspension density.

residence length of the strands. Consequently, as the results presented in Fig. 10 were obtained in our relatively smooth column, the characteristic residence length of the strands plotted in Fig. 12 may not apply to other columns with different internal surface configurations. For instance, an internal surface in the form of a vertical membrane wall is likely to prolong the residence length of the strands, while one in the form of horizontal or spiralling tubes will likely impede the downward flow of the strands and shorten their characteristic residence length.

To support the above argument, a special 0.46 m long transparent column section was constructed with half of its internal surface in the form of a vertical

membrane wall, similar in geometry to the one used in refs. [7, 8]. Visual observation of hydrodynamics at the wall confirmed that particles moving along the membrane wall behave differently from those moving along an unobstructed (smooth) wall. As the membrane wall is formed by joining parallel vertical tubes by narrow fins, the space between the tubes offers some protection for the strand particles against the various factors (e.g. turbulence) which promote dispersion and mixing of the strands. As a result, particles falling along the fins or webs between the tubes tend to sweep downward in the protected region, thus prolonging the characteristic residence length of the strands for a membrane wall.

High-speed cinematography experiments

During the above runs, the hydrodynamics at the middle level of the column in the vicinity of the two probes were also recorded using high-speed cinematography. These films were then analyzed frame by frame to obtain an estimate of the falling velocity of the strands in the wall layer. The numbers of frames taken for individual strands to fall 0.152 m at the wall are tabulated in Table 3 for four area-averaged suspension densities. The corresponding calculated falling velocities of the strands are given in parentheses in Table 3. It is apparent from Table 3 that there exists a rather wide distribution of falling velocities for the strands at all suspension densities. This conclusion is similar to what has been suggested in our discussion of Fig. 10. It seems also from Table 3 that there is no systematic influence of suspension density on the falling velocities of strands. By averaging all the velocities in Table 3, one can obtain 1.26 m s^{-1} as the average falling velocity for the strands at the wall. This compares reasonably well with the 1.62 m s^{-1} obtained above by using the time lag corresponding to the maximum cross-correlation coefficient of profiles 1a and 1b in Fig. 10. It is interesting to note that

Table 3. Frames of film taken for strands to fall 0.152 m and the corresponding calculated falling velocities (in increasing order) at four suspension densities

	Suspension density (kg m^{-3})			
	15.3	28.1	32.0	46.7
	Frames (velocity, m s^{-1})			
	22 (2.77)	30 (2.03)	28 (2.18)	33 (1.85)
	23 (2.65)	30 (2.03)	32 (1.91)	37 (1.65)
	29 (2.10)	34 (1.79)	33 (1.85)	38 (1.60)
	41 (1.49)	36 (1.69)	36 (1.69)	41 (1.49)
	46 (1.33)	43 (1.42)	41 (1.49)	46 (1.33)
	48 (1.27)	51 (1.20)	41 (1.49)	49 (1.24)
	50 (1.22)	58 (1.05)	45 (1.35)	50 (1.22)
	51 (1.20)	59 (1.03)	45 (1.35)	55 (1.11)
	52 (1.17)	68 (0.90)	49 (1.24)	56 (1.09)
	53 (1.15)	70 (0.87)	50 (1.22)	65 (0.94)
	56 (1.09)	72 (0.85)	54 (1.13)	72 (0.85)
	66 (0.92)	96 (0.64)	63 (0.97)	80 (0.76)
Average	44.8 (1.36)	53.9 (1.13)	43.1 (1.41)	51.8 (1.18)
Std Dev.	13.6 (0.62)	20.4 (0.49)	10.1 (0.36)	14.6 (0.34)

Glicksman [2] measured falling velocities at the wall in the range of 1–1.8 m s^{-1} with a video camera by injecting 80 μm sand particles into an upward gas stream in a 100 mm diameter transparent column. Hartge *et al.* [9] reported falling velocities at the wall in the range of 1–1.2 m s^{-1} using an optical probe in a 400 mm diameter circulating fluidized bed with 85 μm FCC particles, while Geldart [10] suggested strand falling velocities of the order of 1 m s^{-1}. Moreover, recent numerical work on the hydrodynamics in circulating fluidized beds by Tsuo [11] also suggests that strand falling velocities are in the range of 1–1.25 m s^{-1}. Our values are clearly in the same range as those determined by other workers using different columns, different particles, and different operating conditions.

CONCLUSION

Heat transfer mechanisms and local hydrodynamics were studied in a cold model circulating fluidized bed. Simultaneous measurements using a heat transfer probe and a capacitance probe show that the sharp peaks in the instantaneous heat transfer coefficients are directly caused by the arrival of particle strands at the probe surface, confirming the important role played by solid particles in the heat transfer process. Furthermore, analyses of the capacitance probe signals indicate that the particle strands possess wide distributions of voidages which vary with the area-averaged suspension density. In addition, cross-correlation results obtained from two vertically-aligned heat transfer probes suggest that there exist characteristic residence lengths for the strands at the wall before they are dispersed. Observations with a simulated membrane section show that strands travel further along fins or webs separating adjacent tubes than when unprotected in a smooth-walled column. A rather wide range of strand falling velocities was also measured, with an average velocity of 1.26 m s^{-1} for the smooth-walled column.

The results obtained here not only help to elucidate the heat transfer mechanisms, but also provide us with valuable information on the hydrodynamics in a circulating fluidized bed. The results are helpful in formulating a heat transfer model for circulating fluidized beds, presented in a separate paper [12].

Acknowledgement—The authors are grateful to the Natural Sciences and Engineering Research Council of Canada and to Energy, Mines and Resources Canada for financial support of this work.

REFERENCES

1. J. R. Grace, Heat transfer in circulating fluidized beds. In *Circulating Fluidized Bed Technology* (Edited by P. Basu), pp. 63–80. Pergamon Press, Toronto (1986).
2. L. R. Glicksman, Circulating fluidized bed heat transfer. In *Circulating Fluidized Bed Technology II* (Edited by P. Basu and J. F. Large), pp. 13–29. Pergamon Press, Toronto (1988).

3. C. M. H. Brereton, Fluid mechanics of high velocity fluidized beds, Ph.D. dissertation, University of British Columbia, Vancouver, Canada (1987).
4. R. L. Wu, C. J. Lim and J. R. Grace, The measurement of instantaneous local heat transfer coefficients in a circulating fluidized bed, *Can. J. Chem. Engng* **67**, 301–307 (1989).
5. R. L. Wu, Heat transfer in circulating fluidized beds, Ph.D. dissertation, University of British Columbia, Vancouver, Canada (1989).
6. B. Herb, K. Tuzla and J. C. Chen, Distribution of solid concentrations in circulating fluidized bed. In *Fluidization VI* (Edited by J. R. Grace, L. W. Shemilt and M. A. Bergougnou), pp. 65–72. Engineering Foundation, New York (1989).
7. R. L. Wu, C. J. Lim, J. Chaouki and J. R. Grace, Heat transfer from a circulating fluidized bed to membrane waterwall surfaces, *A.I.Ch.E. Jl* **33**, 1888–1893 (1987).
8. R. L. Wu, J. R. Grace, C. J. Lim and C. M. H. Brereton, Suspension-to-surface heat transfer in a circulating fluidized bed combustor, *A.I.Ch.E. Jl* **35**, 1685–1691 (1989).
9. E.-U. Hartge, D. Rensner and J. Werther, Solids concentration and velocity patterns in circulating fluidized beds. In *Circulating Fluidized Bed Technology II* (Edited by P. Basu and J. F. Large), pp. 165–180. Pergamon Press, Toronto (1988).
10. D. Geldart, Electric Power Research Institute Workshop on Erosion in Circulating Fluidized Bed Combustors, Argonne, Illinois (1989).
11. Y. P. Tsuo, Computation of flow regimes in circulating fluidized beds, Ph.D. dissertation, Illinois Institute of Technology, Chicago, Illinois (1989).
12. R. L. Wu, J. R. Grace and C. J. Lim, A model for heat transfer in circulating fluidized beds, *Chem. Engng Sci.* (1991), in press.

TRANSFERT THERMIQUE LOCAL INSTANTANE ET HYDRODYNAMIQUE DANS UN LIT FLUIDISE CIRCULANT

Résumé—Les mécanismes locaux de transfert thermique et d'hydrodynamique sont étudiés dans un modèle transparent de lit fluidisé circulant, haut de 9,3 m, de diamètre 152 mm pour du sable d'Ottawa de 171 μm. Des mesures instantanées à la paroi sont faites avec des sondes à transfert thermique couvertes de platine. Dans certaines conditions, des taux de vide sont mesurés avec une sonde à capacitance. Les résultats montrent que les pics soudains et violents dans les coefficients de transfert thermique instantané sont directement causés par l'arrivée de paquets de particules sur la surface de transfert thermique. L'analyse des signaux de la sonde à capacitance indique que ces paquets possèdent une large distribution de vide. Les mesures simultanées de la sonde de transfert thermique suggèrent l'existence de longueurs caractéristiques de résidence de ces paquets. La vitesse moyenne de chute des paquets est évaluée à 1,26 m s^{-1} en utilisant la cinématographie ultrarapide.

MOMENTANES ÖRTLICHES VERHALTEN VON WÄRMEÜBERGANG UND HYDRODYNAMIK IN EINEM ZIRKULIERENDEN WIRBELBETT

Zusammenfassung—In einem transparenten kalten Modellwirbelbett von 9,3 m Höhe, 152 mm Innendurchmesser aus Ottawa-Sand (171 μm) werden der örtliche Wärmeübergang und die Hydrodynamik untersucht. Mit einem platinbeschichteten Wärmeübergangssensor werden Momentanmessungen an der Wand ausgeführt. Unter bestimmten Bedingungen werden mit einer Kapazitätssonde gleichzeitig örtliche Leerstellen festgestellt. Die Ergebnisse zeigen plötzlich auftretende scharfe Spitzen bei den gemessenen momentanen Wärmeübergangskoeffizienten, die unmittelbar durch die Ankunft von Partikelserien an der wärmeübertragenden Oberfläche verursacht werden. Die Analyse der Signale der Kapazitätssonde zeigt eine weite Verteilung von Leerstellen, die sich mit der örtlichen zeit- und flächengemittelten Verteilungsdichte ändert. Die gleichzeitigen Messungen mit dem Wärmeübergangssensor legen die Existenz von charakteristischen Aufenthaltszeiten für diese Partikelserien nahe. Ihre durchschnittliche Fallgeschwindigkeit wird mit Hilfe von Hochgeschwindigkeitsaufnahmen zu 1,26 m s^{-1} bestimmt.

ЛОКАЛЬНЫЙ ТЕПЛОПЕРЕНОС И ГИДРОДИНАМИКА В ЦИРКУЛИРУЮЩЕМ ПСЕВДООЖИЖЕННОМ СЛОЕ

Аннотация—Исследуются механизмы локального теплопереноса и гидродинамика в прозрачном ненагретом модельном циркулирующем слое оттавского песка с размером частиц 171 мкм, высота которого составляет 9,3 м, а внутренний диаметр—152 мм. Мгновенные измерения у стенки проводятся при помощи датчиков теплообмена с платиновым покрытием. Для некоторых условий мгновенная локальная пористость определяется с использованием емкостного зонда. Полученные результаты показывают, что внезапные и ярко выраженные пики в измеренных коэффициентах нестационарного теплопереноса непосредственно обусловлены приближением струй частиц к поверхности теплопереноса. Анализ сигналов емкостного зонда свидетельствует о том, что эти струи характеризуются неоднородной пористостью, которая изменяется с изменением локальной усредненной по времени и площади плотности взвеси. Одновременные измерения с использованием датчика теплопереноса предполагают существование характерных длин для этих струй. При помощи высокоскоростной киносъемки найдено, что средняя скорость стрй равна 1,26 м $с^{-1}$.